Disponible en ligne sur
ScienceDirect
www.sciencedirect.com
Elsevier Masson France
EM|consulte
www.em-consulte.com
IRBM
IRBM 35 (2014) 11–19

Biomedical image segmentation using variational and statistical approaches

Segmentation of the pulmonary vascular trees in 3D CT images using variational region-growing

M. Orkisz [a,*], M. Hernández Hoyos [b], V. Pérez Romanello [b], C. Pérez Romanello [b], J.C. Prieto [a], C. Revol-Muller [a]

[a] *Université de Lyon, CREATIS, CNRS UMR 5220, Inserm U1044, INSA-Lyon, Université Lyon 1, Lyon, France*
[b] *Universidad de los Andes, Grupo Imagine, Grupo de Ingeniería Biomédica, Bogotá, Colombia*

Received 5 July 2013; received in revised form 14 November 2013; accepted 5 December 2013
Available online 30 January 2014

Abstract

Objectives. – The long-term goal of this project is to quantify the aeration of lung parenchyma in 3D CT scans of patients with acute respiratory distress syndrome. This task requires lung delineation, as well as elimination of airways and vessels. The objective of this article was to present and evaluate the method used to segment out the vascular trees.
Materials and methods. – Vascular trees are segmented by variational region growing. This process is performed within a lung mask, where the airways and bronchial walls were previously eliminated by adaptive multi-scale morphological operations. The region growth starts from seeds defined as the most salient points on a "vesselness" map. The "vesselness" function based on the eigenvalues of the Hessian matrix is also used in the region descriptor that controls variational region growing. The formulation of this descriptor, as well as the method used to eliminate the bronchial walls, are the original contributions of this work. The method was evaluated using the full set of 20 chest scans from the VESSEL12 challenge framework.
Results. – Overall specificity of 0.938 and sensitivity of 0.772 were achieved. The method successfully differentiated vessels from bronchial walls (specificity, 0.848) but failed to detect the smallest vessels (sensitivity, 0.418).
Conclusion. – To the best of our knowledge, similar formulations of variational region growing have never been used to segment pulmonary vascular trees. The method seems to be suitable for the intended application, although its validation on actual images with acute respiratory distress syndrome remains to be done.

1. Introduction

Pulmonary vessel analysis from computed tomography (CT) images is an important step in the diagnosis, treatment planning, and follow-up of lung diseases [1]. Since the pulmonary vessel trees are very complex and have a huge number of branches, computerized methods may be helpful to reduce the reader's effort. For example, delineation of vascular trees may simplify the detection of pulmonary emboli on these images by reducing the search space and thus the number of false alerts outside the vascular structures [2]. Differentiation of vasculature from focal opacities is very useful for the detection of lung cancer and other localized pathologies. Quantitative assessment of the vascular tree can also provide important information for the functional understanding of pulmonary anatomy and objective measures of lung diseases [3,4]. For instance, quantitative assessment of artery diameters may determine over distension of a pulmonary artery, an index of pulmonary hypertension [5]. The vascular trees can also serve as a roadmap for the tracking of lung tissues across lung volume changes or across time as the lung is serially monitored [6].

Our interest in the extraction of pulmonary vascular structures is related to a medical research project studying the effects of mechanical ventilation on lung aeration (assessed with CT) in patients with acute respiratory distress syndrome (ARDS). ARDS is defined as intense pulmonary inflammation and hyper-permeability caused by different parenchyma aggressions that

* Corresponding author. Campus LyonTech la Doua - INSA de Lyon, bâtiment Blaise-Pascal, 7, rue Jean-Capelle, 69621 Villeurbanne cedex, France.
E-mail addresses: maciej.orkisz@creatis.insa-lyon.fr (M. Orkisz), marc-her@uniandes.edu.co (M. Hernández Hoyos), juan-carlos.prieto@creatis.insa-lyon.fr (J.C. Prieto), chantal.muller@creatis.insa-lyon.fr (C. Revol-Muller).

1959-0318/$ – see front matter © 2013 Elsevier Masson SAS. All rights reserved.
http://dx.doi.org/10.1016/j.irbm.2013.12.001

can be related to a set of clinical, radiological, and physiological manifestations [7]. The management of patients with ARDS in intensive care units includes the use of mechanical ventilation. However, mortality was consistently estimated around 40% in adults across the last decade [8,9], although a study published in 2008 [10] suggested a slight decrease (1.1% per year). It is estimated that 25% of these deaths might be avoided by better adapting the ventilation parameter settings for these patients. In order to assist the clinicians in setting up ventilation parameters, lung aeration has to be quantified and monitored. In this context, we seek to develop a method to automatically quantify lung aeration in ARDS CT images. This quantification requires a preliminary segmentation of the lung envelope and the elimination of both the airway and blood-vessel trees, in order to only quantify the air contained inside the lung parenchyma. This article focuses on presenting and evaluating the method devised to segment out the pulmonary-vessel tree.

There is a rich literature on 3D vessel enhancement and segmentation methods. To the best of our knowledge, the currently most general and extensive vascular segmentation review can be found in [11], with a highly detailed categorization of the existing work. Most of these techniques focus solely on single-branch segmentation based on the extraction of the centerline of the vessel of interest, which is very useful for display, segmentation, and quantification purposes. Another important category deals with segmentation of simple vascular trees (in terms of the number of ramifications) such as carotid [12] and coronary [13] trees. However, most of these techniques cannot be applied to the pulmonary trees due to their tiny size, complex patterns, and the huge number of ramifications, *e.g.*, a method using a sophisticated geometrical model devised to identify bifurcations and branch terminations [14], can hardly process a whole chest CT in a reasonable time. For these reasons and despite a relatively good contrast with respect to the background, vascular segmentation in the lungs is challenging.

Pulmonary vessel segmentation from CT images has been studied with a focus on different applications. Proposed approaches vary from thresholding operations to front propagation techniques. We refer the readers to [1] and [15] for extensive reviews of pulmonary vessel segmentation methods. Many of the algorithms therein cited are based on the enhancement or detection of tubular structures by computing features from the eigenvalues of the Hessian matrix [3,6,16–19]. This helps better differentiate between vessel and non-vessel regions in the segmentation process.

The method presented in this article also performs a vessel enhancement, prior to the actual vessel tree segmentation. These tasks are carried out in a volume of interest, which is automatically delineated by segmenting the lung envelope and eliminating the airways. The most salient points after the vessel-enhancement process are used as seeds in the final segmentation by variational region growing (VRG). VRG formalism describes region growing as an optimization process that aims to minimize an objective function called energy [20]. While the conventional region growing is based on homogeneity criteria calculated within the region, VRG can include region shape information via an appropriate energy choice.

Section 2 describes the segmentation method in three subsections: the first one summarizes the theoretical background of the main components implemented in this method, the second one explains our contributions devised for the target application, and the third one outlines the data and criteria used to evaluate the method. The results are presented in Section 3, and then a discussion and conclusions are given in Section 4.

2. Methods and materials

Our image-processing pipeline consists of three main steps: delineation of the volume of interest (VOI) where the pulmonary vessel tree will be sought, vessel enhancement, and actual vessel tree segmentation. Fig. 1 represents the overall workflow. The VOI generation involves lung segmentation and bronchi elimination. The most salient points after the vessel-enhancement process carried out within the VOI are used as seeds in the final segmentation by VRG. The lungs and bronchi are segmented using state-of-the art methods that will not be detailed in this article. Lung segmentation is based on thresholding and morphological operations [21], whereas the airway tree is segmented by region growing with leakage detection, introduced by [22], which iteratively increases a threshold value until the number of voxels aggregated in one iteration becomes excessive. We rejected a more complex bronchi-segmentation approach requiring an initial segmentation of the arterial tree. Although this approach is powerful, it is limited to the images acquired after injection of an arterial contrast-agent. Hereafter, we focus on the main contribution, *viz.* an application-adapted implementation of VRG, and then we briefly explain why and how the bronchial wall is removed.

2.1. Background

This section summarizes the theoretical background of the main components implemented in the method. The first subsection describes the general formulation of the VRG approach introduced in [23]. The second subsection outlines how the Hessian matrix eigenvalues are used to enhance thread-like structures such as vessels, by means of so-called "vesselness" (or "tubularness") criteria.

2.1.1. VRG formulation

Let $\Omega \in \mathbb{R}^D$ denote the image domain ($D=3$ for a three-dimensional image), $\Omega_{\text{in}} \in \Omega$ being the currently segmented region and $\Omega_{\text{out}} = \Omega \backslash \Omega_{\text{out}}$ its complement. The region Ω_{in} iteratively evolves toward a minimum of an energy function denoted J. To formulate this energy, the Ω_{in} region is represented by a discrete binary function ϕ such that for a voxel $\mathbf{x} \in \Omega$:

$$\phi(\mathbf{x}) = \begin{cases} 1, & \text{if } \mathbf{x} \in \Omega_{\text{in}} \\ 0, & \text{if } \mathbf{x} \in \Omega_{\text{out}} \end{cases} \quad (1)$$

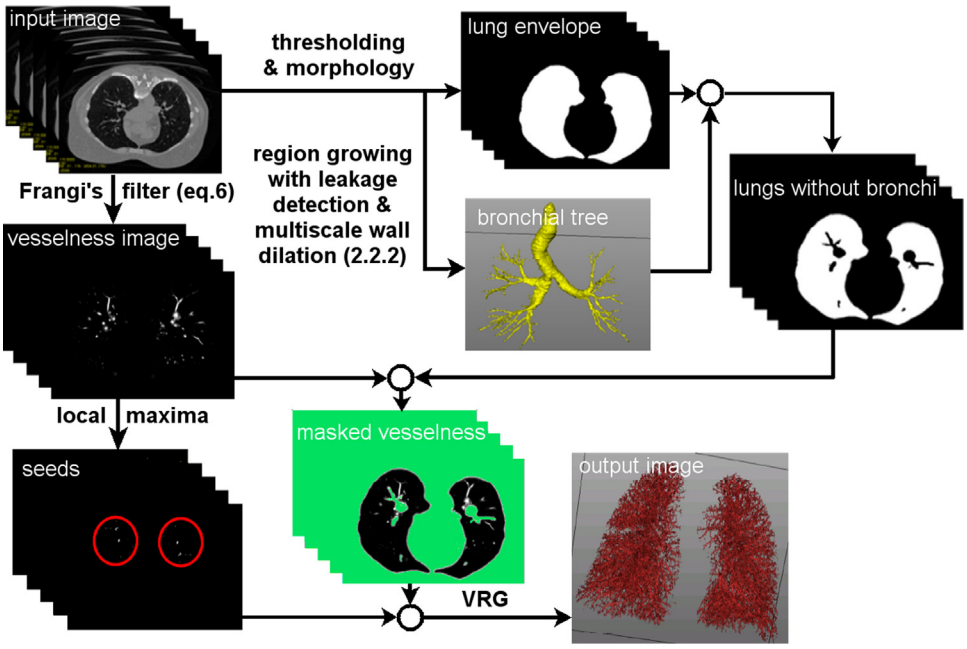

Fig. 1. Overview of the proposed method. From the input image, the lung envelope is segmented out and combined with the result of the bronchial-tree extraction. A "vesselness" image calculated from the input image is used to detect seed-points. Final segmentation of the vascular trees starts from these seeds and extends within the "vesselness" image limited to the lung region.

Using k to denote a region descriptor, *viz.* a function characterizing the voxels expected to belong to Ω_{in}, the total energy at the n-th iteration is equal to [20]:

$$J(\phi^n) = \sum_{\mathbf{x} \in \Omega} k(\mathbf{x})\, \phi^n(\mathbf{x}) \tag{2}$$

Since $\phi^n(\mathbf{x}) = 1$ only at voxels $\mathbf{x}$ belonging to the currently segmented region Ω^n_{in}, Equation (2) is a sum of potentials defined by the function $k(\mathbf{x})$ within this region. Let $\Delta J\left(\phi^{n+1}\right)$ denote the energy variation, such that $J\left(\phi^{n+1}\right) = J(\phi^n) + \Delta J\left(\phi^{n+1}\right)$. At each iteration one candidate voxel $\mathbf{x}$ is considered for aggregation, and it has been demonstrated [23] that the corresponding energy variation is given by:

$$\Delta J\left(\phi^{n+1}(\mathbf{x})\right) = \left(1 - 2\phi^n(\mathbf{x})\right) k(\mathbf{x}) \tag{3}$$

Depending on the sign of this variation, the candidate voxel is aggregated to Ω_{in} if the energy decreases or is rejected otherwise, *viz.* the voxel state switches according to the equation:

$$\phi^{n+1}(\mathbf{x}) = \frac{1}{2}\left(1 - \text{sign}\left(\Delta J\left(\phi^{n+1}\right)\right)\right) \tag{4}$$

The function $k(\mathbf{x})$ needs to be defined such that its values are negative within the structures to be segmented (here vessels) and positive in the background. Equation (3) thus leads to negative values of $\Delta J\left(\phi^{n+1}(\mathbf{x})\right)$ at candidate voxels $\mathbf{x}$ if and only if $k(\mathbf{x})$ is also negative (at candidate voxels, *i.e.*, not yet belonging to Ω^n_{in}, $\phi^n(\mathbf{x}) = 0$). The growth stops when neither of the candidate points can be aggregated or when a maximum number of iterations is achieved. Details can be found in the seminal article, as well as in [24–27], where various specific applications were tackled. Hereafter we will focus on the definition of a region descriptor appropriate for the pulmonary vessel tree segmentation problem. This descriptor is based on the notion of "vesselness" summarized in the next subsection.

2.1.2. *"Vesselness" functions and Hessian eigenvalues*

Without loss of generality, blood vessels in medical images are usually modeled as tubular structures brighter than the surrounding tissues, which is also the case in the present application. Otherwise, image contrast inversion or sign change in formulas would be sufficient to cope with images where vessels appear darker than the background. Under this assumption, the voxels located within a vessel, near its centerline, can be characterized using the second derivatives of the image gray-levels: the derivative along the local vessel orientation should be close to zero, while the derivatives in the cross-sectional plane should have large negative values. However, the local orientation is unknown *a priori*. Therefore, the derivatives are computed according to the axes of the image coordinate system. Then they are put together to build the Hessian matrix $\mathbf{H}(\mathbf{x})$ and the matrix is diagonalized, so that one of its eigenvectors is aligned with the vessel in $\mathbf{x}$, while the remaining ones span the cross-sectional plane. Given that the Hessian eigenvalues $|\lambda_1| \leq |\lambda_2| \leq |\lambda_3|$ correspond to the second derivatives along the eigenvectors, the following configuration is expected at voxels $\mathbf{x}$ located within the vessel:

$$\lambda_3 \approx \lambda_2 \ll \lambda_1 \approx 0 \tag{5}$$

Based on these considerations, several "vesselness" criteria have been proposed in the literature, *i.e.*, [28–31] and are used in vessel-enhancement filters and segmentation algorithms. The derivatives usually are computed by convolving the image with the derivatives of the Gaussian, which offers the possibility of a multi-scale analysis by varying the parameter σ of the Gaussian

to fit the local radii of the vessels. The largest response across the scales is then retained. We selected the Frangi criterion [29], which is the most frequently cited, although there is no formal proof that any of the published criteria systematically outperforms the others. This criterion involves three components: $R_A = |\lambda_2/\lambda_3|$ tends toward 1 in circular cross-sections, $R_B = \lambda_1/\sqrt{|\lambda_2\lambda_3|}$ tends toward 0 in elongated structures, and $S = \|\mathrm{H}\|_F = \sqrt{{\lambda_1}^2 + {\lambda_2}^2 + {\lambda_3}^2}$ is the Frobenius norm of the Hessian used to measure how structured the local content of the image is. The actual expression of the criterion is:

$$\nu = \begin{cases} 0, \text{ if } \lambda_2 > 0 \text{ or } \lambda_3 > 0 \\ \left(1 - \exp\left(-\frac{{R_A}^2}{2\alpha^2}\right)\right) \exp\left(-\frac{{R_B}^2}{2\beta^2}\right) \left(1 - \exp\left(-\frac{S^2}{2c^2}\right)\right), \text{ otherwise,} \end{cases} \quad (6)$$

with recommended parameter values $\alpha = \beta = 0.5$, whereas c needs to be experimentally set depending on the image type considered. Here, we empirically set $c = 500$. The first term tends to 1 at voxels located at the center of circular cross-sections, because the exponent is then close to $-1/\alpha^2$, according to equation (5). Likewise, the second term tends to 1 at voxels located within elongated structures, because the exponent is then close to 0 with $\lambda_1^2 \ll |\lambda_2\lambda_3|$. Finally, the third term is devised to cancel the effect of the previous ones when all the derivatives are small and the configuration $\lambda_3 \approx \lambda_2 \ll \lambda_1 \approx 0$ is due to image noise rather than to the actual presence of a vessel. Let us note that matrix diagonalization at each voxel and at multiple scales is computationally expensive. However, by analyzing matrix invariants, such as trace and determinant, it is possible to reject a large percentage of voxels unlikely to meet the condition (5) without diagonalization [32].

2.2. Methodological contributions

2.2.1. Region descriptor for pulmonary vascular trees

Let us underline that one of the main features, by which VRG differs from conventional region growing, is its capability to incorporate a shape prior via the function k. In our case, the shape is expected to be tubular, *i.e.*, if the seeds are located within vessels, then the voxels belonging to Ω_{in} should be characterized by large values of "vesselness" ν. The value of ν at a candidate voxel $\mathbf{x}$ located in a vessel should be close to the mean value of ν calculated within the vessels segmented thus far (Ω_{in}). Hence, with $\mu_{\nu_{\text{in}}}$ denoting this mean value and $\mu_{\nu_{\text{out}}}$ denoting the mean value of ν within the background Ω_{out}, the difference $\left|\nu(\boldsymbol{x}) - \mu_{\nu_{\text{in}}}\right|$ should be smaller than $\left|\nu(\mathbf{x}) - \mu_{\nu_{\text{out}}}\right|$. Based on these considerations, the region descriptor function was defined as follows:

$$k(\mathbf{x}) = \frac{\nu(\mathbf{x})}{M_\nu}\left(\left|\nu(\mathbf{x}) - \mu_{\nu_{\text{in}}}\right|^2 - \left|\nu(\mathbf{x}) - \mu_{\nu_{\text{out}}}\right|^2\right) + \frac{f(\mathbf{x})}{M_f}\left(\left|f(\mathbf{x}) - \mu_{f_{\text{in}}}\right|^2 - \left|f(\mathbf{x}) - \mu_{f_{\text{out}}}\right|^2\right) \quad (7)$$

As explained above, the expression $\left(\left|\nu - \mu_{\nu_{\text{in}}}\right|^2 - \left|\nu - \mu_{\nu_{\text{out}}}\right|^2\right)$ is expected to take negative values within vessels and positive values outside vessels. We also incorporated a similar expression involving the image intensity function f and its respective mean values in Ω_{in} and Ω_{out}, so as to guarantee the homogeneity of the segmented region. This second term also is negative when $f(\mathbf{x})$ is closer to the mean intensity in vessels $\mu_{f_{\text{in}}}$ than to that in the background $\mu_{f_{\text{out}}}$. Each of these two terms is normalized by the maximum value of the respective function: $M_\nu = \max_{\mathbf{x}\in\Omega}(\nu)$ and $M_f = \max_{\mathbf{x}\in\Omega}(f)$. Their contributions thus have the same magnitude despite a large difference in dynamics between $\nu \in [0, 1)$ (by definition) and $f \in \left[0, 2^L - 1\right]$ (in images coded on L bits).

2.2.2. Elimination of the bronchial wall

As specified in Fig. 1, vessel segmentation by VRG is performed within a lung mask. Although the "vesselness" function was designed to enhance tubular shapes, experimental results demonstrated that some unwanted structures may also be segmented. These are mainly bronchial walls, since pulmonary arteries are anatomically "stuck" to corresponding bronchi and also appear bright in images. Therefore, in some configurations, segmentation by VRG is unable to separate them. To solve this problem, bronchi with their walls need to be removed from the lung mask prior to vessel segmentation. Accurate delineation of the bronchial wall is a difficult task and beyond the scope of this work. Instead, we propose to segment the airway lumen and then to dilate it by a quantity equal to the wall thickness. However, the wall thickness strongly varies from one bronchial generation to another. Large bronchi have thick walls and the thickness decreases as the airway diameter decreases. To handle this variation, we propose a multi-scale strategy, illustrated in Fig. 2. The idea is to dilate thicker branches with larger structuring elements and *vice versa*, without explicitly estimating the diameters of the branches in the segmented airway tree. For this purpose, the algorithm generates several copies of the airway tree. The first copy is dilated with a small structuring element such that the layer added corresponds to the wall thickness of the thinnest bronchi likely to be segmented. The second copy first undergoes a morphological opening with a structuring element whose diameter is equal to the diameter of these thin bronchi, so that the corresponding branches are removed from the tree. One can reasonably assume that the remaining branches recover their initial diameters after the opening operation. This remaining tree is dilated with a structuring element larger than the one used to dilate the first tree, thus adding a thicker layer. Similar processing of the next copy, using larger structuring elements, removes additional branches and adds an even thicker layer to the remaining ones, and so on. Copies of the airway tree thus processed form a family of trees ranging from a complete tree dilated with the smallest structuring element, to a tree having

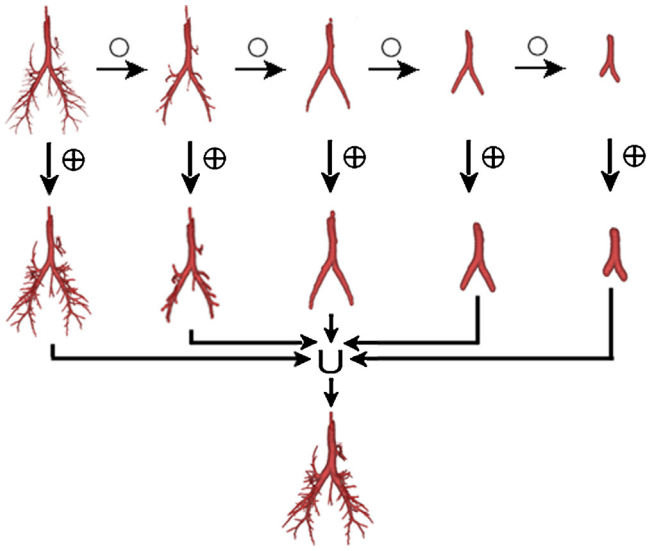

Fig. 2. Multi-scale strategy to construct a mask of the bronchial tree. Starting from the segmented airway lumen, trees with fewer details were obtained by morphological opening with larger structuring elements. Each tree was then dilated with a structuring element whose size was proportional to the radius of the thinnest branches in this tree. The union of all dilated trees covers the airway lumen and walls.

only the thickest branches and dilated with the largest structuring element. Finally, all these trees are combined to build up a single tree. In this combination, the branches present in several trees, and therefore dilated with several different structuring elements, retain the additional thickness corresponding to the largest dilation. A rigorous description of the whole process is provided below.

Let $\mathfrak{A}_0$ denote the initial segmented airway lumen tree. The first step is a series of morphological opening operations with ball-shaped structuring elements $\mathfrak{B}_i^o$. Opening $\mathfrak{A}_0$ with $\mathfrak{B}_i^o$ generates a new tree $\mathfrak{A}_i$, where branches thinner than the diameter of the structuring element $\mathfrak{B}_i^o$ are removed. The radius r_i^o of $\mathfrak{B}_i^o$ progressively increases, $\forall i \in \{1, 2, \ldots, I-1\}, r_i^o < r_{i+1}^o$, and the last tree $\mathfrak{A}_I$ only keeps the largest branches. The second step is a morphological dilation of each tree, using ball-shaped structuring elements $\mathfrak{B}_i^d$. The radius r_i^d of the structuring element $\mathfrak{B}_i^d$ also varies according to the thickness of the thinnest branches in the given tree: $\forall i \in \{0, 1, 2, \ldots, I-1\}, r_i^d < r_{i+1}^d$. In our experiments, we used seven tree levels (*i.e.*, $I = 7$). The radii of the structuring elements used for dilation, expressed in millimeters, were equal to $r_i^d = i + 1, \forall i \in \{0, 1, \ldots, 6\}$ and the corresponding radii used for opening were empirically fixed to be twice as large, *i.e.*, $r_i^o = 2r_i^d = 2(i+1), \forall i \in \{1, 2, \ldots, 6\}$. The final dilated tree is a union of all individually dilated trees: $\mathfrak{A} = \bigcup_{i=0}^{I} \mathfrak{A}_i$.

2.3. Data and evaluation criteria

This method was evaluated using the VESSEL12 framework available online since the corresponding challenge organized in conjunction with the IEEE International Symposium on Biomedical Imaging (ISBI 2012), held in Barcelona, Spain, from 2 to 5 May 2012. All the details about the datasets, reference and evaluation criteria, as well as algorithm descriptions and detailed results obtained by the participating teams, can be found on the VESSEL12 website (vessel12.grand-challenge.org). Here the most important information is summarized.

2.3.1. Datasets

Twenty chest CT scans are available to the users of the framework for evaluation purposes, and three additional scans are provided for training purposes. These scans come from various sources and represent a variety of scanners, imaging protocols, and diseases such as emphysema, nodules, and pulmonary embolisms present in approximately half of the datasets. Also, roughly half of the datasets were acquired after contrast agent injection. The image resolution is nearly isotropic with voxel size ranging from 0.6 to 1.0 mm. Each scan comes with a binary mask of the lung region. The user is free to use these masks if desired, but evaluation is performed only within the non-masked region. Additionally, the training datasets come with annotations.

2.3.2. Reference

The images were annotated by three observers. Since it is intractable to manually delineate all the blood vessels in each complete 3D scan, the annotations were performed in a number of axial slices drawn from each dataset. In each of these slices, the observers were asked to label a large number of points, both local maxima and random, located within the lungs. The points were labeled as either vessel or non-vessel, and within the non-vessel category the following sub-labels were used: lung parenchyma, fissure, airway/airway wall, and lesion. Only the points where the labels of the three observers agreed were retained in the evaluation system. The labels corresponding to the 20 datasets used for evaluation are not available to the framework users.

2.3.3. Evaluation

The framework users submit the entire outcome of their 3D segmentation in a standardized file format. The submitted volumes can be either binary (vessel/non-vessel) or probabilistic (the value at a given voxel should indicate how confident one can be that this voxel actually belongs to a vessel). The evaluation system selects from the submitted volumes the points corresponding to the available reference labels and uses them to calculate a number of metrics based on ROC (receiver operating characteristic) curve analysis. Three measures are used: area under the curve (*AUC*), specificity, and sensitivity. It should be remembered that sensitivity, also called the true-positive rate (*TPR*), is the proportion of true positives (here correctly detected vessels) with respect to the total number of positives (detected and undetected vessels), *i.e.*, true positives (*TP*) and false negatives (*FN*): $TPR = TP/(TP + FN)$. Symmetrically, specificity is the proportion of true negatives (non-vessels detected as such) with respect to the total number of negatives, *i.e.*, true negatives (*TN*) and false positives (*FP*): $SPC = TN/(FP + TN) = 1 - FPR$, where *FPR* is the false-positive rate. Ideally, both *TPR* and *SPC* should be close to 1. In binary submissions, true/false positives/negatives can be directly determined from the submitted volume, whereas in probabilistic submissions, these values

Table 1
Detailed scores from the VESSEL12 evaluation framework: area under ROC curve (*AUC*), specificity (*SPC*), and sensitivity (*TPR*). The overall score is followed by scores for various vessel sizes, and finally by scores showing how well vessels were differentiated from other high-density objects. The first two columns define which voxels were used to calculate the scores, *i.e.*, in the 5th row the positive class includes the voxels labeled as vessels, whereas the negative class only includes the voxels labeled as non-vessel/airway walls. Below each score of our method, the range of scores achieved by all the methods submitted to the challenge is specified.

	Positive points	Negative points	*AUC*	*SPC*	*TPR*
1	All vessel points	All non-vessel points	0.879	0.967	0.772
			0.561–0.986	0.556–0.994	0.165–0.949
2	Points in small vessels	All non-vessel points	0.693	0.957	0.418
			0.425–0.977	0.356–0.995	0.009–0.932
3	Points in medium-sized vessels	All non-vessel points	0.953	0.967	0.918
			0.485–0.986	0.510–0.994	0.020–0.960
4	Points in large vessels	All non-vessel points	0.976	0.981	0.952
			0.709–0.994	0.942–0.994	0.449–0.961
5	All vessel points	Points in airway walls	0.845	0.848	0.772
			0.376–0.944	0.515–0.994	0.097–0.949
6	Vessel points in dense abnormalities (contrast scans)	Non-vessel points in dense abnormalities	0.766	0.561	0.808
			0.612–0.884	0.478–0.996	0.178–0.836
7	All vessel points	Non-vessel points in dense abnormalities	0.583	0.340	0.772
			0.446–0.789	0.291–0.998	0.097–0.949
8	All vessel points	Points in nodules	0.367	0.115	0.772
			0.324–0.731	0.072–0.992	0.097–0.949
9	All vessel points	Points in mucus-filled bronchi	0.495	0.133	0.772
			0.184–0.660	0.133–0.969	0.097–0.949

correspond to the optimal threshold, *i.e.*, the point on the ROC curve closest to the upper left-hand corner of the graph. A ROC curve is a plot representing *TPR vs. FPR* obtained when varying the detection threshold of a binary detector. A perfect detector would achieve $AUC = 1$, whereas a random guess leads to $AUC = 0.5$. To calculate *AUC* for binary submissions, these are automatically transformed to probabilistic submissions by applying a signed distance transform.

In addition to overall results, the values of *AUC*, *SPC*, and *TPR* are calculated separately for each dataset and for several categories aiming to assess the capability of segmenting large, medium-sized and small vessels, and to differentiate vessels from airway walls, mucus-filled bronchi, and dense lesions (*i.e.*, atelectasis, nodules, fibrosis, adhesive straining), respectively.

3. Results

We submitted to the VESSEL12 evaluation framework both binary volumes directly resulting from VRG segmentation, and probabilistic volumes, where each voxel of the segmented vessels was weighted by the corresponding "vesselness" value. The overall results were very similar for both submissions: $AUC = 0.874$, $SPC = 0.938$, $TPR = 0.774$ for the binary submission and $AUC = 0.879$, $SPC = 0.967$, $TPR = 0.772$ for the probabilistic submission. Therefore, herein we only report the detailed results for our probabilistic submission (Table 1). Each score can be compared to the range of scores achieved by all the segmentation methods submitted to the evaluation framework. When analyzing these ranges, one has to keep in mind that very high scores in terms of specificity were almost always achieved by the last-ranked method, which performed very poorly in terms of sensitivity. Conversely, even the overall best-ranked method had the poorest specificity in dense lesions, nodules, and mucus-filled bronchi. Table 2 summarizes the overall scores of each submission. We only included the actual segmentation methods, *i.e.*, those that involve a hard decision on whether or not each voxel considered belongs to a pulmonary vessel. Indeed, based on the information available from the challenge website, one can note that several submissions are not segmentations but only vessel-enhancement results. The organizers were able to evaluate them via ROC curve analysis because they know the reference and are therefore able to find an optimal threshold for each submission. Nevertheless, it does not make much sense to compare these submissions to those where vessels were separated from non-vessels without knowing the reference.

Table 2
Overall scores of the segmentation methods submitted to the VESSEL12 framework. Our method (CreaLung) is ranked fifth.

Rank	Submission name	*AUC*	*SPC*	*TPR*
1	UofA vision	0.986	0.941	0.949
2	FME_LungVessels	0.981	0.953	0.935
3	DIAG	0.932	0.936	0.900
4	NTNU	0.902	0.947	0.842
5	CreaLung	0.879	0.967	0.772
6	BWH-ACIL	0.852	0.924	0.738
7	ARTEMIS-TSP	0.837	0.994	0.680
8	ASBMI	0.812	0.981	0.641
9	TSSeg	0.766	0.920	0.604
10	MedKIS	0.737	0.748	0.591
11	simira	0.671	0.795	0.463
12	Labhuman	0.652	0.556	0.598
13	SU_UT	0.561	0.950	0.165

Compared to the scores of the best-performing method, the present method had very similar specificity, but lower sensitivity, in that it failed to detect a number of small vessels (Fig. 3). Nevertheless, this figure also shows that this method handled

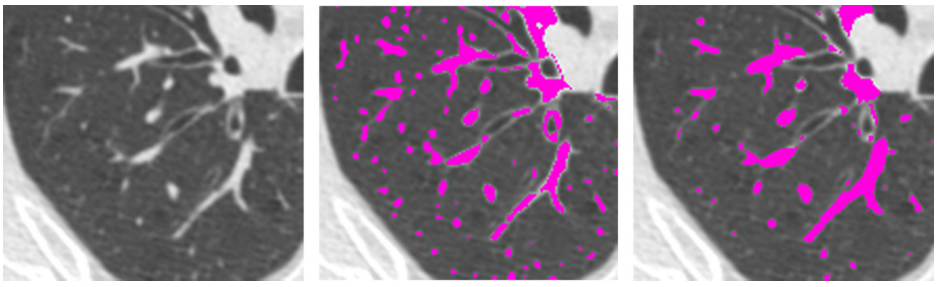

Fig. 3. Small-vessel detection. Fragment of original image slice (left), superposition of segmentation results obtained by the best-performing method (center) and our method (right).

airway walls better, which is confirmed by a lower specificity of the compared method in the vessel *vs*. airway wall category ($SPC = 0.745$, to be compared with row 5 in Table 1). To demonstrate the efficacy of the strategy used to remove the bronchial walls, one can also compare the scores from Table 1 to the results of our method run without the elimination of bronchial walls, in particular: overall $AUC = 0.739$, $SPC = 0.834$, $TPR = 0.555$ (to be compared with row 1 in Table 1), and vessels *vs*. airway walls $AUC = 0.544$, $SPC = 0.877$, $TPR = 0.475$ (to be compared with row 5 in Table 1). Fig. 4 illustrates this improvement. Fig. 5 shows examples of entire vascular trees segmented using our method.

4. Discussion and conclusion

Referring to Table 1, it can be noted that our method achieved good overall specificity, but lower sensitivity (row 1), mainly due to missed small vessels (row 2). Using multi-scale elimination of bronchial walls, the method successfully differentiates vessels from airway walls (row 5). It also detects vessels passing through dense abnormalities fairly well, provided that a vascular contrast agent is used (row 6). In the absence of contrast agent, the specificity of our method significantly drops in the regions where dense abnormalities can be mistaken for vessels (rows 7–9). In particular, mucus-filled bronchi are difficult to differentiate from vessels because they have the same shape, size, and density. Therefore, even the best-performing method from the VESSEL12 challenge achieved poor specificity in this case ($SPC = 0.133$, identical to our method). Interestingly, the best-performing method of the challenge was less specific than ours in regions with dense lesions ($SPC = 0.291$ overall and $SPC = 0.478$ in scans with contrast agent) and nodules ($SPC = 0.072$). The latter observation suggests that our method is likely to be more successful in images of patients with ARDS, in which dense lesions are spread across a large part of the lungs. Additionally, it is not essential to detect all the smallest vessels, as they represent a small percentage of the overall lung volume, and missing a part of them would not severely hamper the quantification.

To the best of our knowledge, although several teams used variational methods in vascular segmentation, none of their

Fig. 4. Airway wall elimination. Example of original slice (left), superposition of segmentation results obtained without (center) and with (right) airway-wall elimination.

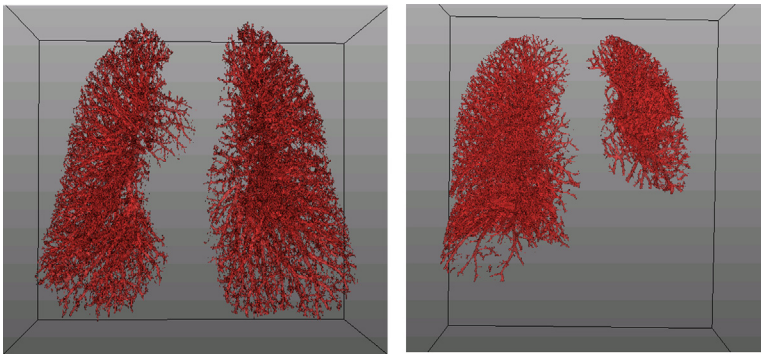

Fig. 5. Examples of vascular trees segmented by our method.

approaches can be directly compared to the VRG algorithm and none has been evaluated on pulmonary images. As an example, let us cite a variational method [33] using fuzzy region competition. Its feasibility was demonstrated on a chest CT scan, among other images, but no evaluation was carried out and the formalism was quite different. Similarly, a variational method evaluated on CT angiography images of the liver [34] is actually not a region-growing technique.

Of the methods submitted to the VESSEL12 evaluation framework, the best-performing one completely differs from the remaining submissions, as it is based on machine learning. The remaining methods share several components, albeit in varying – more or less complex – combinations. Descriptions of two binary submissions are missing on the challenge website. Nevertheless, from the available information one can conclude that approximately half of the submissions in some way used Hessian-based vesselness measurement, mainly Frangi's (at least four submissions, including ours) with different parameter settings. At least four teams, including ours, eliminated the bronchial walls by dilating the previously segmented airway lumen, and one team attenuated them using a level-set approach applied after an explicit estimation of airway diameters. Our method is the only one that uses an adaptive dilation, without explicit estimation of airway diameters.

In conclusion, the method herein described seems to be suitable for the intended application, although validation on actual images with ARDS remains to be done. On images from the VESSEL12 challenge, representing lungs with various pathologies, our method ranked among the five best-performing submissions in the same category.

Acknowledgements

This study was conducted within the framework of the French LABEX PRIMES (ANR-11-LABX-0063) of Université de Lyon, and was partly supported by the following grants: French-Colombian ECOS-Nord #C11S01 and Colombian Colciencias #1204-519-28996.

References

[1] Kaftan JN, Aach T. Pulmonary vessel segmentation for multislice CT data: methods and applications. In: El-Baz A, Suri JS, editors. Lung imaging and computer aided diagnosis. CRC Press; 2011. p. 189–219.

[2] Masutani Y, MacMahon H, Doi K. Computerized detection of pulmonary embolism in spiral CT angiography based on volumetric image analysis. IEEE Trans Med Imaging 2002;21(12):1517–23.

[3] Liu X, Chen DZ, Wu X, Sonka M. Optimal graph-based segmentation of 3D pulmonary airway and vascular trees across bifurcations. Proceedings of MICCAI 1st Int Workshop on Pulmonary Image Processing, New York, USA; 2008. p. 103–11.

[4] Fetita C, Brillet PY, Prêteux FJ. Morpho-geometrical approach for 3D segmentation of pulmonary vascular tree in multi-slice CT. Proceedings of SPIE, Med Imaging: Image Processing, Lake Buena Vista, FL, USA; 2009, p. 72594F-1–11.

[5] Wittram C, Maher MM, Yoo AJ, Kalra MK, Shepard JO, McLoud TC. CT angiography of pulmonary embolism: diagnostic criteria and causes of misdiagnosis. Radiographics 2004;24:1219–38.

[6] Shikata H, McLennan G, Hoffman EA, Sonka M. Segmentation of pulmonary vascular trees from thoracic 3D images. Int J Biomed Imaging 2009. DOI:10.1155/2009/636240, article ID 636240, 11 p.

[7] Bernard GR, Artigas A, Brigham KL, Carlet J, Falke K, Hudson L, et al. Report of the American-European consensus conference on ARDS: definitions, mechanisms, relevant outcomes and clinical trial coordination. The Consensus Committee. Intensive Care Med 1994;20(3):225–32.

[8] Brun-Buisson C, Minelli C, Bertolini G, Brazzi L, Pimentel J, Lewandowski K, et al. Epidemiology and outcome of acute lung injury in European intensive care units. Results from the ALIVE study. Intensive Care Med 2004;30(1):51–61.

[9] Pierrakos C, Karanikolas M, Scolletta S, Karamouzos V, Velissaris D. Acute Respiratory Distress Syndrome: pathophysiology and therapeutic options. J Clin Med Res 2011;4(1):7–16.

[10] Zambon M, Vincent JL. Mortality rates for patients with acute lung injury/ARDS have decreased over time. Chest 2008;133:1120–7.

[11] Lesage D, Angelini ED, Bloch I, Funka-Lea G. A review of 3D vessel lumen segmentation techniques: models, features and extraction schemes. Med Image Anal 2009;13(6):819–45.

[12] Hameeteman K, Zuluaga MA, Freiman M, Joskowicz L, Cuisinaire O, Flórez Valencia L, et al. Evaluation framework for carotid bifurcation lumen segmentation and stenosis grading. Med Image Anal 2011;15(4):477–88.

[13] Kirişli HA, Schaap M, Metz C, Dharampal AS, Meijboom WB, Papadopoulou SL, et al. Standardized evaluation framework for evaluating coronary artery stenoses detection, stenoses quantification and lumen segmentation algorithms in computed tomography angiography. Med Image Anal 2013;17(8):859–76.

[14] Carrillo JF, Hernández Hoyos M, Dávila Serrano EE, Orkisz M. Recursive tracking of vascular tree axes in 3D medical images. Int J Comput Assist Radiol Surg 2007;1(6):331–9.

[15] Sluimer I, Schilham A, Prokop M, van Ginneken B. Computer analysis of computed tomography scans of the lung: a survey. IEEE Trans Med Imaging 2006;25(4):385–405.

[16] Lo P. Segmentation of lung structures in CT. PhD thesis. University of Copenhagen; 2010.

[17] Zhou C, Chan HP, Sahiner B, Hadjiiski LM, Chughtai A, Patel S, et al. Automatic multiscale enhancement and segmentation of pulmonary vessels in CT pulmonary angiography images for CAD applications. Med Phys 2007;34(12):4567–77.

[18] Zhou C, Chan HP, Kuriakose JW, Chughtai A, Hadjiiski LM, Wei J, et al. Computerized detection of pulmonary embolism in computed tomographic pulmonary angiography (CTPA): improvement of vessel segmentation. Proceedings of SPIE, Med Imaging: Computer-Aided Diagnosis, Lake Buena Vista, FL, USA; 2011, p. 79630L-1–9.

[19] Xiao C, Staring M, Shamonin D, Reiber JH, Stolk J, Stoel BC. A strain energy filter for 3D vessel enhancement with application to pulmonary CT images. Med Image Anal 2011;15(1):112–24.

[20] Jehan-Besson S, Barlaud M, Aubert G. DREAM2S: deformable regions driven by an Eulerian accurate minimization method for image and video segmentation. Int J Comput Vision 2003;53(1):45–70.

[21] Hu S, Hoffman EA, Reinhardt JM. Automatic lung segmentation for accurate quantitation of volumetric X-ray CT images. IEEE Trans Med Imaging 2001;20(6):490–8.

[22] Mori K, Hasegawa J, Suenaga Y, Toriwaki J. Automated anatomical labeling of the bronchial branch and its application to the virtual bronchoscopy system. IEEE Trans Med Imaging 2000;19(2):103–14.

[23] Rose JL, Revol-Muller C, Reichert C, Odet C. Variational region growing. Proceedings of VISAPP, Lisboa, Portugal. 1; 2009. p. 53–6.

[24] Rose JL, Revol-Muller C, Charpigny D, Odet C. Shape prior criterion based on Tchebichef moments in variational region growing. Proceedings of ICIP, Cairo, Egypt; 2009. p. 1081–4.

[25] Rose JL, Grenier T, Revol-Muller C, Odet C. Unifying variational approach and region growing segmentation. Proceedings of EUSIPCO, Aalborg, Denmark; 2010. p. 1781–5.

[26] Pacureanu A, Revol-Muller C, Rose JL, Sanchez-Ruiz M, Peyrin F. A vesselness-guided variational segmentation of cellular networks from 3D micro-CT. Proceedings of ISBI, Rotterdam, Netherlands; 2010. p. 912–5.

[27] Revol-Muller C, Grenier T, Rose JL, Pacureanu A, Peyrin F, Odet C. Region growing: adolescence and adulthood; two visions of region growing: in feature space and variational framework. Proceedings of VISAPP, Rome, Italy; 2012. p. 286–97.
[28] Sato Y, Nakajima S, Shiraga N, Atsumi H, Koller T, Gerig G, et al. Three-dimensional multi-scale line filter for segmentation and visualization of curvilinear structures in medical images. Med Image Anal 1998;2(2):143–68.
[29] Frangi AF, Niessen WJ, Hoogeveen RM, van Walsum T, Viergever MA. Model-based quantitation of 3D magnetic resonance angiographic images. IEEE Trans Med Imaging 1999;18(10):946–56.
[30] Li Q, Sone S, Doi K. Selective enhancement filters for nodules, vessels, and airway walls in two- and three-dimensional CT scans. Med Phys 2003;30(8):2040–51.
[31] Zhou C, Chan HP, Chughtai A, Patel S, Hadjiiski LM, Wei J, et al. Automated coronary artery tree extraction in coronary CT angiography using a multiscale enhancement and dynamic balloon tracking (MSCAR-DBT) method. Comput Med Imaging Graph 2012;36(1):1–10.
[32] Orlowski P, Orkisz M. Efficient computation of Hessian-based enhancement filters for tubular structures in 3D images. Innov Tech Biol Med 2009;30:128–32.
[33] Mory B, Ardon R, Thiran JP. Variational segmentation using fuzzy region competition and local non-parametric probability density functions. Proceedings of 11th ICCV, Rio de Janeiro, Brazil; 2007. DOI: 10.1109/ICCV.2007.4408959.
[34] Freiman M, Joskowicz L, Sosna J. A variational method for vessels segmentation: algorithm and application to liver vessels visualization. Proceedings of SPIE Medical Imaging; 2009. DOI: 10.1117/12.810611.